CrossMark

Specific Measurements of In-Flight Droplet and Particle Behavior and Coating Microstructure in Suspension and Solution Plasma Spraying

P. Fauchais, M. Vardelle, S. Goutier, and A. Vardelle

The plasma spraying of suspensions of sub-micro- or nano-sized particles and of solutions of chemicals precursors produces finely structured coatings that have generally enhanced properties compared to conventional plasma-sprayed coatings. However, most techniques used in conventional plasma spraying are no more adapted to experimentally observe the behavior of the liquid feedstock in the plasma jet and investigate the effect of the operating conditions on liquid fragmentation in droplets, solid particles released by solvent evaporation or formed from the chemical precursors. Also, specific techniques have to be used to study the coating formation and characterize its microstructure. This paper aims to present the main techniques developed or adapted, up to now, to study the plasma-liquid feedstock interactions and characterize the coatings achieved by suspension and solution plasma spraying.

1. Introduction

Under suspension and solution plasma spray conditions, the formation of plasma-sprayed coatings from particles finer (a few hundred nanometers to a few micrometer in diameter) than particles used in conventional plasma spraying (10 to 100 μm in diameter) compels to adapt or even develop specific techniques to characterize the behavior of droplets and particles within the plasma jet and microstructure of the resulting coatings. These techniques are necessary to understand better the suspension plasma spray (SPS) and solution precursor plasma spray (SPPS) processes and tailor the spray conditions to achieve coatings meeting the specifications of given applications.

The aim of this paper is to take stock of the main techniques used up to now that for some were specifically adapted to SPS and SPPS: It will begin with the characterization of void architecture and mechanical properties of plasma-sprayed sub-micro- or nano-structured coatings and, then, present the main techniques used to investigate in-flight the droplet size and velocity distribution as well as

the sub-micrometer-particle temperatures, velocities, and trajectories.
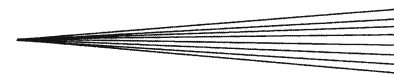
2. SPS and SPPS Coating Characterizations

The behavior of coatings under mechanical and thermal loading depends on their thermal, thermo-elastic, plastic, and fracture properties. The latter are affected by the void architecture (void network) of the coatings which is controlled by the operating conditions of the spray process and substrate parameters that govern coating formation.

2.1 Void Architecture

The features of the void network involve the void global content or porosity, void size distribution, shape of voids (globular, more or less elongated, cracks...), and void network connectivity (Ref 1, 2). The stereological protocols that make it possible to statistically extrapolate the three-dimensional material from representative plane sections of coating are not adapted when the characteristic dimension of voids is below 0.1 μm. Also the methods used to measure the coating porosimetry as Archimedean porosimetry, mercury intrusion porosimetry, and electrochemical methods are not suited. However, three methods could be used with nanometer-sized suspension plasma-sprayed coatings; they are (i) gas (generally helium) pycnometry to quantify the open void content of coatings; this technique does not present any relevant drawback and has been successfully implemented on nanometer-sized suspension plasma-sprayed coatings, (ii) small angle neutron

P. Fauchais, M. Vardelle, S. Goutier, and A. Vardelle, SPCTS-UMR CNRS 7315, University of Limoges, Limoges, France. Contact e-mail: pfauchais@gmail.com.

scattering (SANS); it enables the characterization of the void network features including surface area distribution and orientation distribution (Ref 1, 2); however, it has not been implemented yet for SPS and SPPS coatings to the best of our knowledge and (iii) ultra-small angle x-ray scattering (USAXS), similar to SANS, recording elastic scattering of x-rays induced by compositional and structural inhomogeneity; this nondestructive technique has been successfully implemented; e.g., the void size distribution was investigated in yttria-stabilized zirconia (YSZ) suspension plasma-sprayed coatings with a suspension mean size (d_{50}) of 50 nm (Ref 3) and it was found that about 80% of voids, in number, exhibited characteristic dimensions smaller than 30 nm, the largest voids being few hundred nanometers.

2.2 Mechanical Properties

For conventional plasma-sprayed coatings, a popular test is micro-indentation that gives the hardness (H) and elastic modulus (E) of coatings. The former is a measure of the quasi-static resistance to deformation and the latter is a measure of coating stiffness. SPS and SPPS coatings are made of splats with a diameter below 3-2 μm and thickness of a few tenths of μm; they contain small pores between splats and exhibit areas with different hardnesses, unmolten or partially melted particles with sizes below 1-2 μm and pores corresponding to softer areas. Nano-indentation is mandatory to characterize such coatings (Ref 4). The indentations, which location is followed by optical microscopy, are performed on polished cross sections as the coating surface is relatively too rough for nano-indentation measurements. H and E are deduced from the load-depth penetration. Gross and Saber-Samandari (Ref 4) concluded that this tool, they tested on SPS hydroxyapatite coatings, was a valuable tool for the assessment of the mechanical properties in solid areas of porous materials, and was useful for the further development of SPS coatings. Bannier et al. (Ref 5) used this technique to demonstrate that the addition of titania to alumina SPS coatings caused different crystalline phases and improved the powder melting rate which led to higher hardness and elastic modulus. Also Carpio et al. (Ref 6) used nano-indentation to study the effect of operation spray parameters onto YSZ SPS coating microstructure and mechanical properties.

3. Plasma-Liquid Feedstock Interactions

The liquid may be fed to the plasma flow under the form of a liquid stream, blobs or droplets, depending on the injection system. When the system used for liquid injection supplies a liquid stream, the latter undergoes first a primary break-up caused by the plasma cross flow. The resulting drops or droplets may then undergo a secondary breakup depending on the ratio between the deforming inertial forces and stabilizing cohesive forces exerted on the droplets, represented by the Weber number.

3.1 Liquid-Plasma Interaction

When injecting the liquid within the plasma jet core, where temperatures are over about 8000 K, pictures taken with short shutter times (10^{-4} s for example) along different angles, such as orthogonal or parallel to the injector axis, showed the fast cooling of the jet. The plasma jet was cut into two parts where the liquid jet was mechanically injected (Ref 7), before it became again symmetrical downstream. To characterize the effect on the plasma temperature the plasma computer tomography (PCT) developed by Landes (Ref 8) can be used. Examples of the measurements achieved with this technique are given in the papers of Mauer et al. (Ref 9) and Schein et al. (Ref 10) for a plasma jet issuing from a three-cathode segmented anode TriplexPro™ plasma torch.

Another problem to account for is the plasma voltage fluctuations, resulting in variations of the plasma jet core length and velocity, especially with plasma forming gases containing di-atomic gas. Investigating the correlation between the time of liquid injection and further treatment requires time-resolved imaging (Ref 11) with a camera triggered by the instantaneous plasma torch voltage. To follow the cold liquid penetration in the hot highly radiating plasma flow, the latter must be illuminated with laser or arc lamp. For example Etchart-Salas et al. (Ref 11) used a fast shutter camera coupled with a laser sheet flash of 2 μs at 808 nm, the image acquisition being triggered when the arc voltage reached a given threshold. Figure 1(a) illustrates the penetration of the suspension jet (ethanol solvent) within the plasma jet, which voltage fluctuated between 40 and 100 V with a period of about 200 μs. The picture was taken for an instantaneous arc voltage of 65 V, corresponding to the mean voltage. The distance between the mechanical injector and plasma jet was such that the liquid jet started to form droplets 300 μm in diameter before penetrating the plasma with a velocity of 26.6 ± 2 m/s. Several individual clouds of liquid and/or solid within the plasma jet could be clearly identified in Fig. 1(a). Each "cloud" was composed of a compact head of suspension and behind it, some sort of tail with tiny droplets and/or solid particles (Ref 11). The different "clouds" of liquids observed, with heads equally spaced and penetrated in the flow at different times, about 30 μs apart for a laser flash of 2 μs. Figure 1(b) shows the interaction with plasma jet for a low triggering level of 40 V. The liquid jet, insufficiently illuminated by the laser, is represented by a white straight line: no drops can be observed at the plasma jet axis position as they have penetrated into the plasma 100 μs before this picture was taken, i.e., during the preceding half period characterized by higher mass enthalpy, temperature, and velocity. Thus these clouds were swept downstream by the preceding puff of plasma.

To observe the mean trajectories of the materials (liquid and particles) within the plasma flow several images (about 10), taken in the same conditions, can be superposed after eliminating the plasma luminosity (Ref 11). Figure 2 illustrates the results for two plasma jets: relatively low fluctuating Ar-He plasma jet and highly
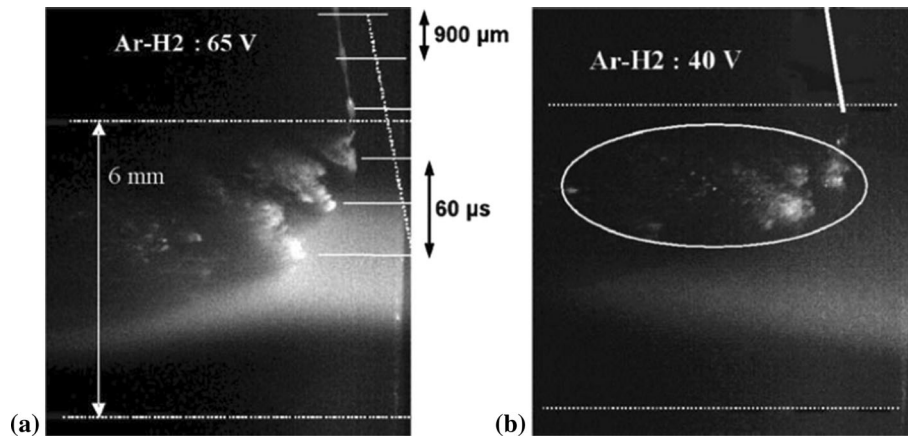
Fig. 1 Observation of the interaction plasma and suspension according to triggering level. Injection velocity of 26.6 m/s, distance between the injector tip and torch axis of 20 mm, Ar-H$_2$ (45-15 slm) gas mixture, anode-nozzle i.d. of 6 mm and arc current of 503 A. (a) triggering level of 65 V, (b) triggering level of 40 V (Ref 11)
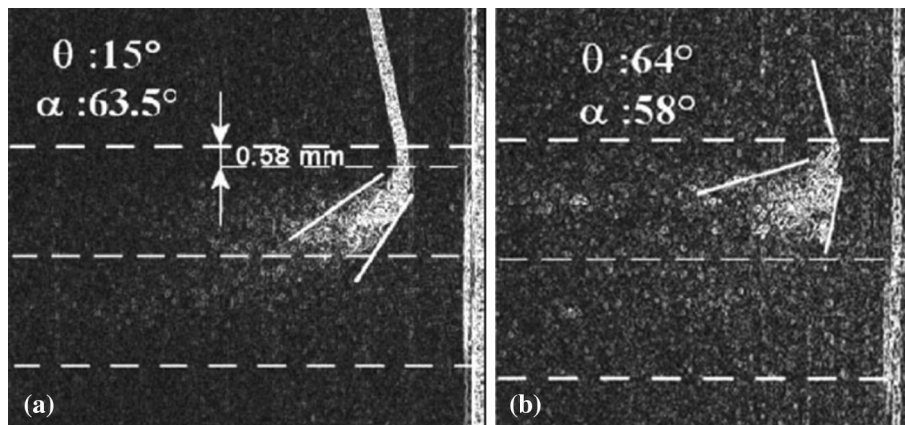

Fig. 2 Interaction between plasma and suspension with an injection velocity of 26.6 m/s, distance between the injector tip and the torch axis of 20 mm: (a) low voltage level of Ar/He (30-30 slm) plasma, anode-nozzle i.d. of 6 mm, arc current of 701 A, (b) high voltage level of Ar/H$_2$ plasma (Ref 11)

fluctuating Ar-H$_2$ one (see Fig. 1 caption for spray conditions). Figure 2(a) shows that with the low fluctuating plasma the droplet dispersion was not very broad: the dispersion angle θ was 15° and the deviation angle of the suspension jet, caused by the momentum of the plasma jet was α = 63.5°. With the highly fluctuating Ar-H$_2$ plasma, Fig. 2(b), the deviation angle θ = 64° was much higher, while the dispersion angle was not so different α = 58°.

Pictures superposition with laser illumination have also been used to characterize the effect of the mean Weber number of the plasma flow on the suspension dispersion within the plasma jet (Ref 12).

Other measurements were developed to characterize the effect of solvent on the plasma jet. Soysal and Ansar (Ref 13) used infrared (IR) images of the vapors emitted by the solvent to characterize the effect of liquid injection. The camera (exposure time of 35 μs) detected radiation from 1.5 to 5 μm and averaged pictures made of 100 single snapshots were observed. Figure 3 presents the signal

obtained along the plasma jet axis emitted by the plasma alone (pure Argon) and when water, ethanol and pentanol are injected in the plasma jet. Compared to the original Ar plasma jet, water and ethanol injections cooled it rather fast, while with ethanol or pentanol the maxima observed in the plasma plume probably came from the post-atomization combustion. This combustion can take place only outside the hot plasma plume when temperatures are below 3000 K. The broad combustion peak of pentanol, higher than that of ethanol, is due to the higher combustion energy of the former. It should be recalled that with SPS or SPPS, the substrate stand-off distances generally range between 35 and 60 mm downstream of the plasma torch when using conventional plasma torches.

Vassen et al. (Ref 14) and Mauer et al. (Ref 15) obtained similar results by using an enthalpy probe to characterizing the plume of plasma jets. They used a Triplex II plasma torch working with an arc current of 500 A, electric power of 56.2 kW, and gas mixture of
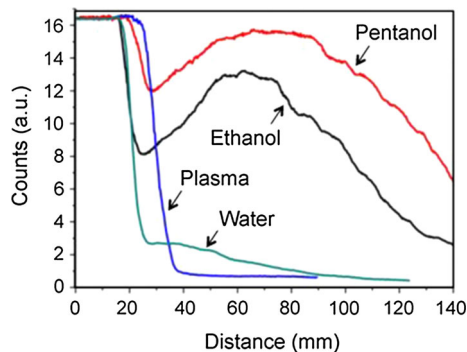
Fig. 3 Line profile along the plasma axis of averaged infrared images (500 A, 50 slm Ar, 20 slm) of pure Ar plasma where water, ethanol or pentanol jets are injected (Ref 13)
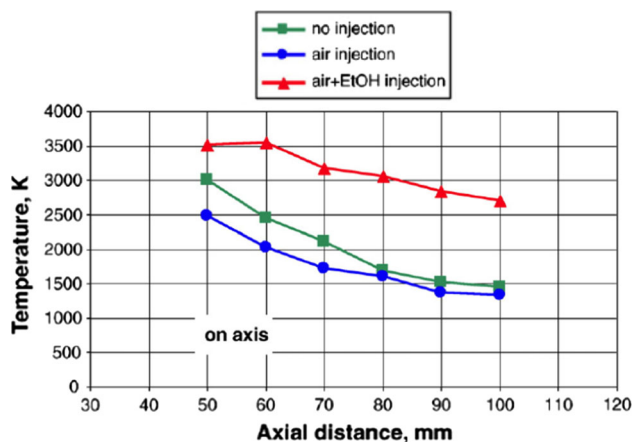

Fig. 4 Axial distribution of measured plasma gas temperatures for three cases, (a) without any injection (no injection), (b) injection of air without ethanol (air injection), and (c) two-phase injection of ethanol and air (air + ethanol injection) (Ref 14)

50 slm Ar and 4 slm He. A typical result is presented in Fig. 4 with no gas or liquid injection, air injection, and air + ethanol injection. It shows that air injection cooled down the plasma plume while the injection of ethanol enhanced noticeably the temperatures in the plasma plume. However, the enthalpy probe could not be used in the too-hot plasma jet core.

3.2 Droplets or Particles In-Flight

As shown previously, the injection of a suspension in a plasma jet core results in its shortening due to liquid vaporization that cools it down. This cooling is about the same with water or ethanol injection but the series of events occurring when injecting the suspension in the plasma jet core will depend on the solvent used. Indeed the liquid surface tension plays an important role in liquid fragmentation, as illustrated schematically in Fig. 5 for a plasma jet obtained with a stick-type cathode torch. With ethanol as solvent, the primary and secondary break-ups of drops and vaporization of the resulting droplets are achieved rather fast, the released particles being acceler-
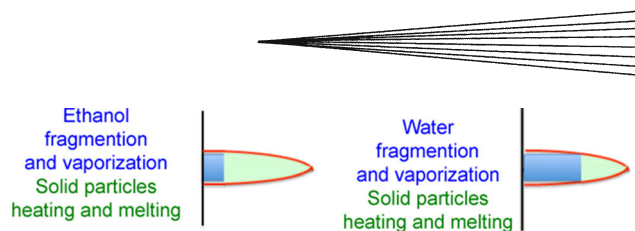

Fig. 5 Schematic of the liquid fragmentation and vaporization followed by released solid particles heating and melting
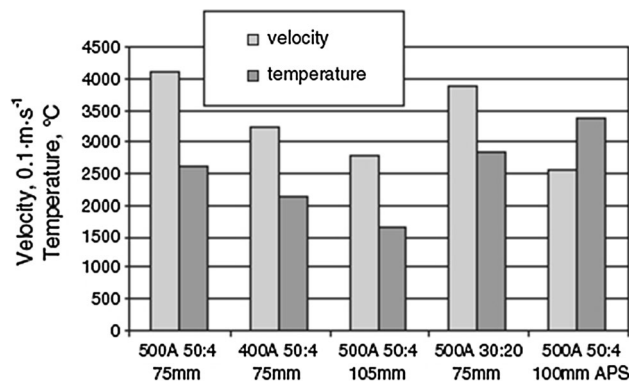

Fig. 6 Velocities and temperatures of droplets in the SPS process for different plasma arc currents (500 and 400 A, gas mixtures of Ar/He (50-4 and 30-20 slm) and stand-off distances (75 and 105 mm) (Ref 14)

ated, heated and melted in the green zone shown in Fig. 5. With water, the Weber number is lower as its surface tension is higher and the fragmentation of drops and droplets occurs along distances that can be twice longer or more than with ethanol. It must be pointed out that in the blue zone shown in Fig. 5, the droplet velocities increased and will control to a large extent the final velocities of the solid particles released by solvent evaporation. When using water as solvent the length of the area where solid particles were accelerated, heated, and melted was shorter. For a better understanding of the phenomena, the drop and droplet sizes and velocities in the blue zone and particle velocities and temperatures in the green zone should be measured.

For particles or droplets, roughly below 5 µm in diameter, it is, up to now, not possible to proceed to individual particle measurements as done in conventional plasma spraying with for example the DPV 2000 system (Tecnar Automation, Canada) but ensemble particle velocity and temperature measurement can be used (Ref 14-18); e.g., in-flight particle parameters were measured at the substrate stand-off distance by using the Accuraspray-g3 system (Tecnar Automation, Canada). In these experiments, the measurement volume consisted of an approximate cylindrical chord, of few tens of mm^3, through the spray pattern and no attempt was made to distinguish between individual particles. Figure 6 presents the results obtained by Vassen et al. (Ref 14) for an ethanol suspension of YSZ particles with sizes below 1 µm sprayed with a Triplex II plasma torch working with Ar-He plasma.
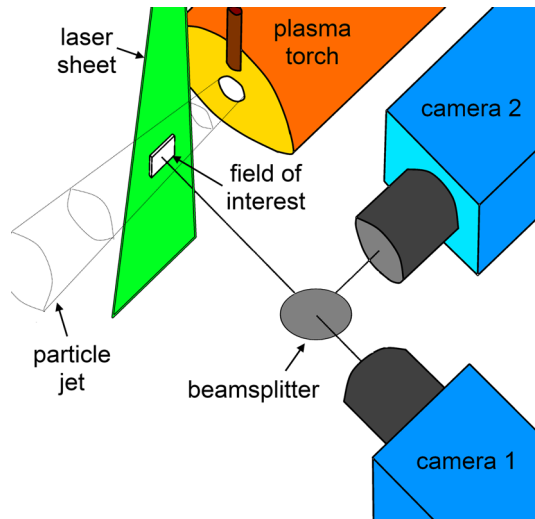
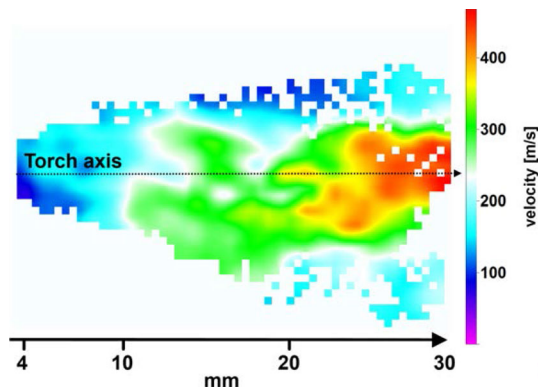**Fig. 7** Experimental test bench of PIV technique for liquid feedstock investigation in plasma jet (Ref 21)

Fig. 8 PIV calculated velocity vector field for the following plasma conditions: Ar 30 slm-H_2 10 slm, $I = 600$ A, anode-nozzle i.d. of 6 mm (Ref 21)

According to the low inertia of particles, once the liquid was evaporated, their ensemble velocity decreased with the spray distance, as their temperature. Higher velocities were achieved with high argon and low helium flow rates contrarily to what is obtained in conventional plasma spraying. The increase in particle temperature with spray distance for the condition characterized by an arc current of 500 A, gas mixture of 50 slm Ar, and 4 slm He is difficult to explain. Such measurements are rather tricky and their validity can be questionable. For example Marchand et al. (Ref 19) have used the Accuraspray system and particle image velocimetry (PIV) method with the same suspension and spray conditions; they found a maximum velocity of 440 m/s with Accuraspray and 210 m/s with PIV. Such a gap gives rise to a questioning on the measurement field and the entities that were investigated.

PIV is a well-established technique for the measurement of the spatial distribution of velocity of various entities (droplets, particles...) in fluid flows (Ref 20) and is used to perform measurements in multi-phase flows: gas-liquid and solid-fluid. Figure 7 shows a PIV system used for the observation of suspension and solution jets in plasma flows; the lighting of the measuring volume was done from the top with a thin and narrow laser sheet to enhance the laser diffusion on the drops or particles and decrease the size of the measurement volume. This PIV-system involved a double-pulsed Nd:YAG laser and two CCD cameras typically 12 bits per pixel with a matrix resolution of 1376×1040 pixels. They were equipped with Nikon AF micro Nikkor 200 mm f/1.4D lens coupled with optical converters (up to 2) and an optical low-pass filter (band pass edge at 578 nm, band width 30 nm). The size of the measurement area ranged between 2 mm × 3 mm and 30 mm × 35 mm. The velocity of a given droplet was measured by following its movement over a specific time. Dedicated software sought, in a given area, droplets with the same diameter in the two images taken by the two cameras (Ref 21).

The PIV technique made it possible to measure, at the end of the blue zone of Fig. 5, the mother droplet velocities and then in the green zone of the plasma jet core the velocity distributions of the released and accelerated particles ($d_p < 1$ µm) (Ref 22). Figure 8 presents the velocity vector field inferred from the PIV image of the whole spray jet with an ethanol suspension. It can be seen that the velocity increased along the torch axis from 150 m s^{-1} at 10 mm of the nozzle exit up to 450 m s^{-1} at 30 mm. A more precise evaluation of particle velocity required increasing the lens magnification by a factor of about 10 to achieve 2 mm × 3 mm measuring area. The optimum standoff distance could be, thus, determined from the axial variation of the mean velocity, as shown in Fig. 9 for two spray conditions.

The shadowgraph technique was also used; it is based on high-resolution imaging with pulsed backlight illumination (Ref 23) to visualize liquid jet and droplets within the plasma jet and determine droplet number and size and, also particle velocity in a given measuring volume. The measuring volume is defined by the optical parameters of the imaging system (focal length and depth of field). The main advantage of this technique is the possibility to work on single entities and independently measure the size and velocity of droplets and particles with different optical characteristics (transparent or opaque). The minimal size that can be measured depends on the imaging system and light source; it is generally a few micrometers. An example is presented in Fig. 10 where the light source was a double-pulsed Nd:YAG laser (wavelength 532 nm, repetition rate 15 Hz, pulse duration 4 ns, pulse energy 800 mJ) equipped with an optical diffuser. The double-pulse laser combined with two cameras (12 bits per pixel, matrix resolution 1376×1040 pixels) equipped with Nikon AF micro Nikkor 200 mm f/1.4D lens coupled with optical converters (up to 2) and an optical low-pass filter (band pass edge at 578 nm, band width 30 nm) allowed the investigation of droplet velocity. The wavelength of the optical filter was slightly different from that of the laser because of the characteristics of the

optical diffuser. The velocity of a given droplet was measured by following its movement over a specific time. The measured data are treated with dedicated software
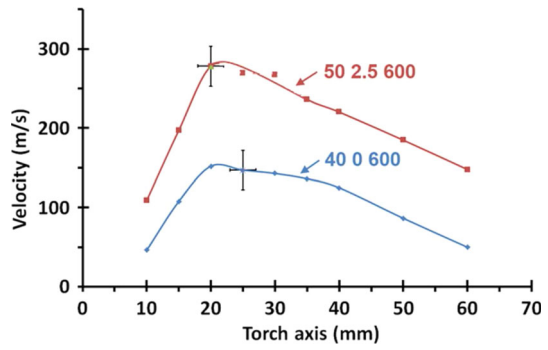

Fig. 9 Variation of particle velocity along the plasma torch axis for two plasma gas mixtures: Ar 40 slm and Ar 50 slm-H$_2$ 2.5 slm, $I = 600$ A, anode-nozzle i.d. of 6 mm. PIV measurement area: 2×3 mm^2 (Ref 21)
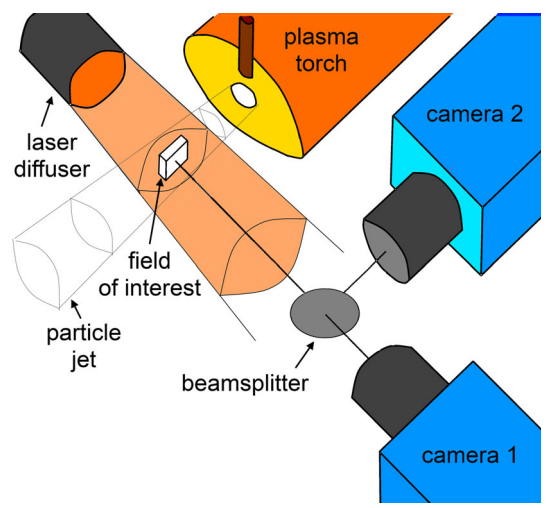

Fig. 10 Experimental test bench for shadowgraph technique (Ref 21)

(Davis 8, developed by LaVision GmbH, Germany). For more details see (Ref 21).

The shadowgraph technique enables the observation of the onset of the liquid jet primary and secondary fragmentations and their locations within the plasma jet, as illustrated in Fig. 11.

Figure 12 shows what happens to in-flight drops and droplets according to the solvent used in the suspension, as it was schematized in the blue zones of Fig. 5.

4. Coating Formation

The first entity to consider in coating formation is the splat resulting from the conversion of impacting particle kinetic energy into work of viscous deformation and surface energy and the substrate thermo-mechanical properties, temperature, roughness, cleanliness (presence or not of adsorbates and condensates), etc. As for conventional coatings, substrate preheating over the transition temperature is mandatory for the coating quality (Ref 1). Contrarily to what is performed in conventional spraying it is, up to now, impossible to measure the diameter and temperature of the impacting particle as well as following
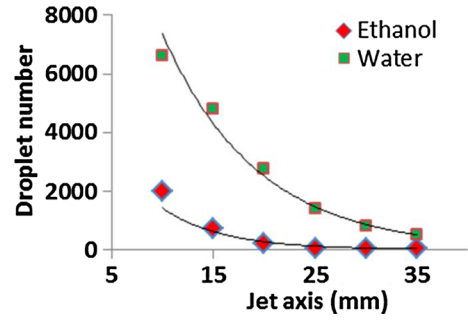
Fig. 12 PIV measurements: variation along the torch axis of droplet number: Plasma spray conditions: Ar 33 slm H$_2$ 10 slm and arc current: 600 A, same injector for the water-base and ethanol-based suspensions and same injection velocity (Ref 21)
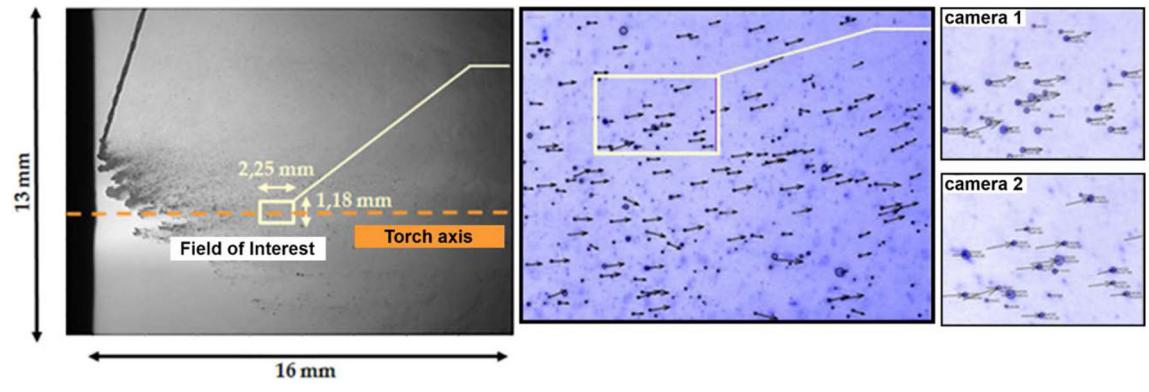

Fig. 11 Observation of the liquid jet break-up by the crossflow plasma jet by using the shadowgraph technique. Resulting velocity vector field at 8 mm from the nozzle exit in a measuring area of 2.25 mm $\times$ 1.18 mm. Plasma spray conditions: Ar 33 slm + H$_2$ 10 slm, $I = 600$ A, suspension injection velocity: 33 m/s (Ref 21)

them during its flattening (Ref 1). The only parameters that can be measured are the diameter of splats collected on different surfaces fixed or mobile and their thickness when using focused ion beam microscopy (destructive method). The in-flight parameter that can be associated to such measurements is the mean velocity of impacting molten particles measured by PIV. According to the lower kinetic energy of the sub-micrometer molten droplets the flattening factor is smaller (<2) than that of the micrometer-sized droplets. It is also worth to note that the quenching of the cooling splats results in much less cracks or no cracks in the corresponding splats.

Another important information can be obtained with the beads formed in SPS or SPPS when moving the torch or the substrate in one direction, also called line-scan experiment (Ref 2). With this technique, the degree of melting of particles, which have traveled in the plasma jet fringes or have been ejected from the high temperature gradient zones of the plasma core can be evaluated. Two regions can be generally identified in spray beads: (i) adherent deposit and, (ii) powdery deposit for SPS (Ref 23, 24) or muddy deposit for SPPS (Ref 25). The observation of the cross sections of beads overlapped or not by using scanning electron microscopy (SEM) allows studying the effect of the spray parameters and efficiency of cooling systems (generally air jets) to eliminate part of the poorly treated particles.

At last, SEM pictures of coatings make it possible to optimize the spray pattern to avoid powdery layers between successive passes (Ref 25).

5. Conclusions

It took almost 50 years to conventional plasma spraying to transform it from an art to a science. Important progress was made when laboratories developed measuring techniques to follow sprayed particles in-flight and at impact. Part of these techniques was later transformed into sensors able to work in the harsh environment of spray booths, which have helped to increase the coating quality. For SPS and SPPS, which are more complex processes, academic research made numerous advances over the last 15 years, especially in the observation of the interactions between the liquid feedstock and plasma jet and of the in-flight parameters of fine (<1 μm) particles. They have contributed to a better understanding of the following phenomena:

(i) The mechanisms that control the interactions between the high-enthalpy plasma flow and liquid drops or jet through the experimental observation of droplets or released particles in-flight.

However, up to now, the sizes of particles or droplets below about 5 μm have not been measured under plasma spray conditions, and ensemble temperature measurements seem to be not very precise. Velocity measurements of very small particles are, however, possible with PIV technique.

(ii) The mechanisms of formation of coating architectures thanks to specific measurements for coating void network and mechanical properties and the study of splats, beads and spray pattern.

However, the optimization of the spray operating parameters has shown that the deposition efficiency is still below about one-third of that of conventional plasma spraying. This could/should require the development of dedicated plasma torches, with higher powers to compensate for energy lost in liquid vaporization, and specifically adapted to the processing of liquids (Ref 2).

References

1. P. Fauchais, J. Heberlein, and M. Boulos, *Thermal Spray Fundamentals*, Springer, Berlin, 2014 (1560pp)
2. P. Fauchais, G. Montavon, R.S. Lima, and B.R. Marple, Engineering a New Class of Thermal Spray Nano-Based Microstructures from Agglomerated Nanostructured Particles, Suspensions and Solutions: An Invited Review, *J. Phys. D*, 2011, **44**, p 093001
3. A. Bacciochini, F. Ben-Ettouil, E. Brousse, J. Ilavsky, G. Montavon, A. Denoirjean, S. Valette, and P. Fauchais, Quantification of Void Network Architectures of As-Sprayed and Aged Nanostructured Yttria-Stabilized Zirconia (YSZ) Deposits, *Surf. Coat. Technol.*, 2010, **205**, p 683-689
4. K.A. Gross and S. Saber-Samandari, Revealing Mechanical Properties of a Suspension Plasma Sprayed Coating with Nanoindentation, *Surf. Coat. Technol.*, 2009, **203**, p 2995-2999
5. E. Bannier, M. Vicent, E. Rayón, R. Benavente, M.D. Salvador, and E. Sánchez, Effect of TiO₂ Addition on the Microstructure and Nano-mechanical Properties of Al₂O₃ Suspension Plasma Sprayed Coatings, *Appl. Surf. Sci.*, 2014, **316**, p 141-146
6. P. Carpio, E. Rayón, L. Pawłowski, A. Cattini, R. Benavente, E. Bannier, M.D. Salvador, and E. Sánchez, Microstructure and Indentation Mechanical Properties of YSZ Nanostructured Coatings Obtained by Suspension Plasma Spraying, *Surf. Coat. Technol.*, 2013, **220**, p 237-243
7. J. Fazilleau, C. Delbos, V. Rat, J.-F. Coudert, P. Fauchais, and B. Pateyron, Phenomena Involved in Suspension Plasma Spraying Part 1: Suspension Injection and Behaviour, *Plasma Chem. Plasma Proc.*, 2006, **26**(4), p 371-391
8. K. Landes, Diagnostics in Plasma Spraying Techniques, *Surf. Coat. Technol.*, 2006, **201**, p 1948-1954
9. G. Mauer, R. Vaßen, and D. Stöver, Plasma and Particle Temperature Measurements in Thermal Spray: Approaches and Applications, *J. Therm. Spray Technol.*, 2011, **20**(3), p 391-406
10. J. Schein, M. Richter, K.D. Landes, G. Forster, J. Zierhut, and M. Dzulkor, Tomographic Investigation of Plasma Jets Produced by Multielectrode Plasma Torches, *J. Therm. Spray Technol.*, 2008, **17**(3), p 338-343
11. R. Etchart-Salas, V. Rat, J.F. Coudert, P. Fauchais, N. Caron, K. Wittman, and S. Alexandre, Influence of Plasma Instabilities in Ceramic Suspension Plasma Spraying, *J. Therm. Spray Technol.*, 2007, **16**(5-6), p 857-865
12. E. Meillot, D. Damiani, S. Vincent, C. Caruyer, and J.P. Caltagirone, Analysis by Modeling of Plasma Flow Interactions with Liquid Injection, *Surf. Coat. Technol.*, 2013, **220**, p 149-156
13. D. Soysal and A. Ansar, A New Approach to Understand Liquid Injection into Atmospheric Plasma Jets, *Surf. Coat. Technol.*, 2013, **220**, p 187-190
14. R. Vaßen, H. Kaßner, G. Mauer, and D. Stöver, Suspension Plasma Spraying: Process Characteristics and Applications, *J. Therm. Spray Technol.*, 2010, **19**(1-2), p 219-225
15. G. Mauer, A. Guignard, R. Vaßen, and D. Stöver, Process Diagnostics in Suspension Plasma Spraying, *Surf. Coat. Technol.*, 2010, **205**, p 961-966
16. F. Tarasi, M. Medraj, A. Dolatabadi, J. Oberste-Berghaus, and C. Moreau, Effective Parameters in Axial Injection Suspension Plasma Spray Process of Alumina-Zirconia Ceramics, *J. Therm. Spray Technol.*, 2008, **17**(5-6), p 685-691
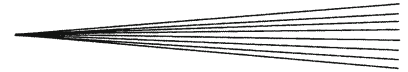
17. O. Tingaud, P. Bertrand, and G. Bertrand, Microstructure and Tribological Behavior of Suspension Plasma Sprayed Al$_2$O$_3$ and Al$_2$O$_3$-YSZ Composite Coatings, *Surf. Coat. Technol.*, 2010, **205**, p 1004-1008

18. F. Tarasi, M. Medraj, A. Dolatabadi, J. Oberste-Berghaus, and C. Moreau, Phase Formation and Transformation in Alumina/YSZ Nanocomposite Coating Deposited by Suspension Plasma Spray Process, *J. Therm. Spray Technol.*, 2010, **19**(4), p 787-795

19. O. Marchand, L. Girardot, M.P. Planche, P. Bertrand, Y. Bailly, and G. Bertrand, An Insight into Suspension Plasma Spray: Injection of the Suspension and Its Interaction with the Plasma Flow, *J. Therm. Spray Technol.*, 2011, **20**(6), p 1310-1320

20. M. Raffel, C.E. Willert, S. Wereley, and J. Kompenhans, *Particle Image Velocimetry: A Practical Guide*, 2nd ed., Springer, Berlin, 2007

21. S. Goutier, J. Varin, W. Duarte, A. Joulia, and M. Vardelle, Laser Diagnostic Techniques for Suspension and Solution Plasma Spraying, in *ITSC 2014 proc.* (*pub.*) DVS Düsseldorf, 2014, p 634-640

22. P. Fauchais, M. Vardelle, S. Goutier, and A. Vardelle, Key Challenges and Opportunities in Suspension and Solution Plasma Spraying, Plasma Chemistry Plasma Processing, Accepted (2015)

23. O. Tingaud, A. Grimaud, A. Denoirjean, G. Montavon, V. Rat, J.-F. Coudert, P. Fauchais, and T. Chartier, Suspension Plasma-Sprayed Alumina Coating Structures: Operating Parameters Versus Coating Architecture, *J. Therm. Spray Technol.*, 2008, **17**, p 662-670

24. P. Fauchais, R. Etchart-Salas, V. Rat, J.-F. Coudert, N. Caron, and K. Wittmann-Ténèze, Parameters Controlling Liquid Plasma Spraying: Solutions, Sols, or Suspensions, *J. Therm. Spray Technol.*, 2008, **17**, p 31-59

25. L. Xie, E.H. Jordan, N.P. Padture, and M. Gell, Phase and Microstructural Stability of Solution Precursor Plasma Sprayed Thermal Barrier Coatings, *Mater. Sci. Eng. A*, 2004, **381**, p 189-195

Peer Reviewed